Atmos. Chem. Phys. Discuss., 14, 14399–14438, 2014
www.atmos-chem-phys-discuss.net/14/14399/2014/
doi:10.5194/acpd-14-14399-2014

Atmospheric Chemistry and Physics Discussions

Comparison of in-situ FISH measurements of water vapor in the UTLS with ECMWF (re)analysis data

A. Kunz[1], N. Spelten[2], P. Konopka[2], R. Müller[2], R. M. Forbes[3], and H. Wernli[1]

[1]Institute for Atmospheric and Climate Research, ETH Zurich, Zurich, Switzerland
[2]Institut für Energie- und Klimaforschung: Stratosphäre (IEK-7), Forschungszentrum Jülich, Jülich, Germany
[3]European Centre for Medium-Range Weather Forecasts, Reading, UK

Received: 2 April 2014 – Accepted: 20 May 2014 – Published: 3 June 2014

Correspondence to: A. Kunz (anne.kunz@env.ethz.ch)

Published by Copernicus Publications on behalf of the European Geosciences Union.

Abstract

An evaluation of water vapor in the UTLS in the atmospheric ERA-Interim reanalysis data set is presented by using in-situ measurements from a large set of airborne measurement campaigns from 2001 to 2011 in the tropics, midlatitudes and polar regions. Water vapor measurements are derived from the Fast In-situ Stratospheric Hygrometer (FISH) and cover isentropic layers from 300–400 K (5–18 km). At the same time, the improvement of the ECMWF assimilation scheme representation of water vapor is addressed for time periods representing different cycles of the Integrated Forecast System (IFS).

The ratio $\Delta(H_2O) = H_2O_{ERA}/H_2O_{FISH}$ is used as a simple measure for the difference between observations and the reanalyses. Overall, the reanalysis data reproduce around 87 % of all FISH measurements within $\Delta(H_2O) = 0.5$–2, and 30 % are within $\Delta(H_2O) = 1.0 \pm 0.1$. Nevertheless, also strong over- and underestimations occur both in the troposphere and in the stratosphere. $\Delta(H_2O)$ values indicate deviations of factors up to 10, with lower deviations in the stratosphere ($\Delta(H_2O) = 0.5$–4) than in the troposphere ($\Delta(H_2O) = 0.5$–10). In the tropical stratosphere the ratio is closer to 1 ($\Delta(H_2O) = 0.5$–2) than in the extratropical stratosphere where strong deviations occur ($\Delta(H_2O) = 0.1$–4).

When considering operational analysis data, the agreement with FISH improves over the time, in particular when comparing water vapor fields for time periods before 2004 and after 2010. It appears that influences of tropical tropospheric and extratropical lower stratospheric processes on the water vapor distribution in the UTLS are particularly challenging, resulting in an overestimation of low and underestimation of high water vapor mixing ratios.

ACPD
14, 14399–14438, 2014

1 Introduction

Water vapor is the number one greenhouse gas in the atmosphere and plays a key role in the atmospheric part of the climate system. A change in water vapor, in particular in the upper troposphere and lower stratosphere (UTLS), affects the surface climate and is important for understanding the decadal variability of surface temperatures (Forster and Shine, 1997; Solomon et al., 2010; Riese et al., 2012).

Water vapor is an extremely variable trace gas that is affected by phase transitions from and to liquid and solid hydrometeors. In the UTLS, the formation and sublimation of ice particles in cirrus clouds is particularly relevant. Water vapor is also involved in atmospheric chemistry. In the troposphere it is the prime source of hydroxyl radicals (e.g., Rohrer and Berresheim, 2006) and thus indirectly controls the lifetime of most gaseous atmospheric pollutants in the atmosphere. In the stratosphere water vapor may be produced through methane oxidation (Jones and Pyle, 1984; Röckmann et al., 2004; Rohs et al., 2006). Transport processes in the troposphere play a key role for the distribution of water vapor. In the vicinity of the tropopause and in particular across the subtropical jet stream large gradients of water vapor exist due to the barrier effects of the tropopause (Haynes and Shuckburgh, 2000; Pan et al., 2004; Flentje et al., 2007; Kunz et al., 2011b). In the tropics, the low temperatures at the tropopause additionally lead to a strong freeze-drying (Jensen and Pfister, 2004; Fueglistaler et al., 2009; Schiller et al., 2009). The representation of these UTLS processes is challenging for operational numerical weather prediction (NWP) models. Thus assimilated and forecasted UTLS water vapor fields might in cases deviate significantly from independent in-situ observations.

One of the most sophisticated NWP models is operated by the European Centre for Medium-Range Weather Forecasts (ECMWF). Besides the operational analysis and forecast cycles, ECMWF has produced different global atmospheric reanalysis products, e.g., ERA-Interim covering the time period from 1979 to near-real time (Dee et al., 2011). ERA-Interim has less data assimilation problems than the former reanalysis

ACPD
14, 14399–14438, 2014

product ERA-40 (Uppala et al., 2006), which were mainly related with the representation of the stratospheric circulation, the quality in stratospheric circulation, and the consistency in time of reanalyzed geophysical fields. Although the observational network changes over time, the reanalysis product is based on a single fixed version of data assimilation and forecast model, in contrast to the changing operational forecasting system.

ERA-Interim water vapor data has been used for studies of key atmospheric processes in the UTLS such as the Brewer–Dobson circulation and double tropopauses (Castanheira et al., 2012), or the transport of water vapor from the subtropics toward the extratropics (Ploeger et al., 2013). Mainly the analysis ECMWF water vapor fields may also be important for flight planning during international aircraft campaigns, e.g., for predicting the occurrence of cirrus clouds. An assessment of the quality of the ERA-Interim water vapor product is therefore relevant for further improving the hydrological cycle in the ECMWF model and for a better understanding and interpretation of diagnostic studies using water vapor fields of this comprehensive data set.

Several validation studies of ECMWF water vapor fields exist in the literature. Flentje et al. (2007) evaluated the short-term high resolution ECMWF forecasts by airborne lidar water vapor measurements during the international TROCCINOX campaign. Based on a case study for March 2004 above the tropical and subtropical Atlantic between Brazil and Europe, Flentje et al. (2007) found an overall good reproduction of the observed water vapor distribution. However, locally there were large differences in the vicinity of strong water vapor gradients and a too moist and shallow boundary layer connected with an overestimation of convective transport. Another analysis by Schäfler et al. (2010) presented a similar case study for operational ECMWF analyses based on measurements during a campaign over western Europe in August 2007. Their comparison of lidar water vapor measurements with ECMWF analyses revealed that the analyses overestimate boundary layer moisture in localized regions over Europe.

A more climatological evaluation of water vapor fields based on the multi-year MOZAIC (Measurements of Ozone and Water Vapour by Airbus In-Service Aircraft)

ACPD
14, 14399–14438, 2014

program was presented for the former ERA-40 data set by Oikonomou and O'Neill (2006) and for operational ECMWF analysis fields by Luo et al. (2007). Oikonomou and O'Neill (2006) found for 1991 to 1999 that the ERA-40 mixing ratios of water vapor are considerably larger than observed by MOZAIC, typically by 20 % in the tropical upper troposphere, and by more than 60 % in the lower stratosphere in high latitudes. The moist bias with an overestimation of the extratropical lower stratospheric specific humidity in the ECMWF operational analysis and forecast system has been also intensively studied with CARIBIC (Civil Aircraft for the Regular Investigation of the atmosphere Based on an Instrument Container) in-situ measurements between 2005 and 2012 (Dyroff et al., 2014). A moist model bias in the extratropical lowermost stratosphere has the potential to impact the temperature distribution including a cold bias near the tropopause (Stenke et al., 2008). It is thus important to improve the moist bias in atmospheric models for radiative fluxes, particularly in the stratosphere where absolute humidities are small, but relative errors can be large. The moist model bias analyzed with the MOZAIC measurements may be due to limitations in the ECMWF model, as described by Oikonomou and O'Neill (2006). Anyhow, the exact difference between the model and MOZAIC measurements may well be influenced by the bias in the MOZAIC water vapor observations in the lower stratosphere. The MOZAIC relative humidity sensor has likely a positive bias above the tropopause, compared to high-resolution observations with the Fast In-situ Stratospheric Hygrometer (FISH) (Kunz et al., 2008).

In the following, all available high-resolution in-situ water vapor measurements by the FISH instrument from 2001 to 2011 are used for a comprehensive assessment of ERA-Interim water vapor in the UTLS. The ECMWF operational analyses are also considered. FISH has successfully participated in a large number of airborne measurement campaigns both in the northern and Southern Hemisphere during recent years. Data from different measurement campaigns are obtained in polar regions (EUPLEX2003, POLARCAT2008, RECONCILE2010), in midlatitudes (SPURT2001–2003, ENVISAT2002, EUPLEX2003, CIRRUS2003–2006, MACPEX2011), and in the tropics

ACPD
14, 14399–14438, 2014

(TROCCINOX2005, SCOUT2005, AMMA2006). All these campaigns had different scientific objectives. Polar campaigns such as RECONCILE2010 aimed at a better understanding of polar vortex dynamics and chemical reactions (von Hobe et al., 2013). Other campaigns, such as the eight SPURT campaigns over two years intended to observe seasonal differences of various trace gases in the midlatitude tropopause region (Engel et al., 2006), and tropical campaigns such as TROCCINOX2005 investigated the impact of tropical deep convection on the distribution and the sources of trace gases, cloud and aerosol particles in the UTLS (Flentje et al., 2007; Schiller et al., 2009).

Taking the water vapor data of all these measurement campaigns therefore results in a comprehensive data set, referred to here as the FISH-based water vapor climatology, at altitudes from 5 to 18 km, i.e., covering the UTLS. A one-to-one comparison of measured and assimilated water vapor fields will be presented for the measurement flights between 2001 and 2011. This comparison will lead to (1) a quantification of the agreement between observed and reanalyzed water vapor for specified episodes, and (2) an investigation of the change of the water vapor representation in operational ECMWF analyses.

The paper is structured as follows. In Sect. 2 the data base will be described. The FISH measurements, the ERA-Interim and the operational analysis data sets will be introduced and the methodology to compare observations and (re)analyses will be described. The results will be presented in Sect. 3 and finally summarized and discussed in Sect. 4.

ACPD
14, 14399–14438, 2014

2 Data description and analysis methodology

2.1 FISH measurements

2.1.1 Measurement technique of FISH

H_2O mixing ratio is measured in-situ using the FISH (Fast In-Situ Stratospheric Hygrometer) instrument (Zöger et al., 1999), which is based on the Lyman α photofragment fluorescence technique. The FISH instrument has been flown on a variety of airborne platforms. It has a forward facing inlet and measures total water, i.e., the sum of the gaseous and the condensed phase. FISH is regularly calibrated in the laboratory against a commercial frostpoint hygrometer. The response time is 1 s, which allows also the detection of small-scale variations of the H_2O mixing ratio in the vicinity of the tropopause, in clouds and contrails. The instrument's accuracy is 6–8 % in the range from 4–100 ppmv and the detection limit is better than 0.3 ppmv at low mixing ratios. The FISH instrument is therefore particularly suitable for water vapor measurements in the stratosphere where other instruments such as the MOZAIC sensors may lose their sensitivity (Kunz et al., 2008). In all aircraft campaigns the FISH instrument is switched on above a pressure level of roughly 400 hPa. The boundary layer is therefore not captured by the FISH measurements. In the lower troposphere, the measurement cell of FISH becomes optically dense due to large mixing ratios and the FISH fluorescence method is limited on in-situ measurements above a mixing ratio of 500 ppmv. Critical FISH measurements above 500 ppmv are therefore excluded from this analysis following Kunz et al. (2008).

2.1.2 FISH-based water vapor climatology

For this study we use the data of ten international measurement campaigns with different scientific objectives and measurement regions (see Table 1 for an overview). The resulting FISH-based water vapor climatology extends from 2001 to 2011. It consists

ACPD
14, 14399–14438, 2014

of measurements from 148 flights on 136 different days corresponding to more than 600 h with FISH water vapor data in the UTLS. In this study, only the gas-phase water vapor is used. In contrast to the Northern Hemisphere airborne in-situ climatology by Tilmes et al. (2010) from 1995 to 2008, only FISH measurements will be considered here, leading to a more homogeneous observational data set based on the same measurement technique.

Figure 1 (top panel) shows the geographical distribution of all measurements included in the FISH-based water vapor climatology. Most of the flights were performed over Europe spanning a region from 30° to 80° N and 10° W to 30° E. In the Northern Hemisphere, the data set also contains measurements over Greenland obtained in 2008, over the US sampled in 2011 and over Africa in 2006. In the Southern Hemisphere, the FISH-based water vapor climatology contains measurements over Brazil and Australia in the year 2005. The highest frequency of measurements is in the vicinity of the tropopause (Fig. 1, bottom panel), roughly around 16 to 18 km in the tropics and around 9 to 12 km in the midlatitudes poleward of the subtropical jet stream. In the Arctic, there is also a high frequency of measurements in the deeper stratosphere at around 18 km from campaigns with polar vortex related objectives such as RECONCILE2010. There is also a high measurement frequency in the middle troposphere at around 5 km from POLARCAT2008.

2.2 ERA-Interim data

The ERA-Interim water vapor product by the ECMWF (Dee et al., 2011) is evaluated in this paper. The model configuration is based on 60 model hybrid levels with the top of the atmosphere located at 0.1 hPa and a spectral T255 horizontal resolution. ERA-Interim is based on IFS release Cy31r2, taken for operational forecasting at ECMWF from 12 December 2006 until 5 June 2007.

Several modifications of the model physics prior to the IFS release Cy31r2 may have a potentially significant impact on the representation of the hydrological cycle. A revised cloud scheme including a new parameterization with supersaturation with respect to ice

ACPD
14, 14399–14438, 2014

in cloud-free parts at temperatures lower than 250 K (Tompkins et al., 2007) is used. The introduction of ice supersaturation delays the formation of ice clouds (Tompkins et al., 2007). Changes of ice sedimentation, cloud-top entrainment, cumulus subsidence, conversion of supersaturated profiles, cloud erosion, and the numerics of the cloud scheme were implemented (Dee et al., 2011). The representation of orographic effects on the atmospheric flow was also refined for ERA-Interim and a modification was made to the atmospheric boundary condition for moisture at the ocean surface to account for salinity effects. At the same time the convection scheme was revised and a new moist boundary-layer scheme based on eddy diffusion combined with mass-flux transport is used which leads to an improved representation of cloud cover (Köhler et al., 2011). Dee et al. (2011) gives a comprehensive overview on the ERA-Interim data set, including the data assimilation methodology, the forecast model, and the input observations.

For this study, ERA-Interim data on a $1^\circ \times 1^\circ$ horizontal grid are used for the 136 days of measurement flights (Table 1 and Fig. 1). The data is then processed as follows:

1. Interpolation of the ERA-Interim specific humidity field to the positions (latitude, longitude, altitude) of the FISH measurements. The temporal interpolation is done by using back- and forward trajectories calculated with the trajectory module of the Chemical Lagrangian Model of the Stratosphere (e.g., McKenna et al., 2002; Ploeger et al., 2013) and transforming the latitude and longitude position of the synoptic observation to the closest analysis times, i.e., 00:00, 06:00, 12:00, and 18:00 UTC. Vertical interpolation is linear in potential temperature. This allows a one-to–one comparison with measured water vapor fields. The ERA-Interim specific humidity values (in $\mathrm{kg\,kg^{-1}}$) are converted to water vapor volume mixing ratio (in ppmv) by multiplication with the quotient of molar masses of dry air and water, i.e., $28.9644/18.015 \times 10^6$.

2. Vertical interpolation of the ERA-Interim meteorological fields, i.e., zonal wind, meridional wind, temperature and geopotential height, on isentropic surfaces

ACPD
14, 14399–14438, 2014

between 280 and 500 K (every 10 K). Afterward, the isentropic static stability, the potential vorticity and the equivalent latitude fields are calculated to further determine the distance of the measurement position on isentropes from the dynamic tropopause based on PV-gradients following Kunz et al. (2011a, b).

3. ERA-Interim temperature fields are extracted in the entire vertical column of the measurement positions. According to WMO (1957) the location of the thermal tropopause based on the vertical lapse rate is determined and the measurement location is also placed in relation with the location of the thermal tropopause on altitude levels.

2.3 Operational analysis data

The same procedure as for the ERA-Interim data in Sect. 2.2 is repeated for the operational analyses. The T511L61 operational analysis data are used from 2001 to 2006. In 2006, the model resolution was increased and accordingly the T799L91 data are retrieved for the later period until 2011. These data are interpolated to a regular $1^\circ \times 1^\circ$ horizontal grid. From 2001 to 2011 there have been multiple model changes from IFS Cycle 23r4 in June 2001, that had been used as cycle for the former reanalysis product ERA-40, to Cycle 37r3 in November 2011. The comparison of the operational analysis water vapor with the FISH observations will therefore be performed in six different time intervals from 2001 to 2011 (see Table 2) according to the information on the web http://old.ecmwf.int/research/ifsdocs/. Each of these time intervals represents almost two years.

2.4 Ratio of water vapor between (re)analysis fields and FISH

After the interpolation of the ECMWF water vapor to the measurement location, the ratio of the ECMWF water vapor is calculated, e.g., the reanalysis water vapor H_2O_{ERA},

ACPD
14, 14399–14438, 2014

and the measured FISH water vapor, H_2O_{FISH}:

$$\Delta(H_2O_{ERA}) = H_2O_{ERA}/H_2O_{FISH}\,. \quad (1)$$

A value of $\Delta(H_2O_{ERA}) = 1$ indicates a perfect agreement between ERA-Interim and FISH, and $\Delta(H_2O_{ERA}) > 1$ indicates an overestimation and $\Delta(H_2O_{ERA}) < 1$ an underestimation of the observed water vapor content. Equation (1) is also applied to the operational analysis water vapor H_2O_{ANA} and the correspondent ratio is referred to as $\Delta(H_2O_{ANA})$ in the following.

2.5 An example flight

Figure 2 shows an example flight path during the MACPEX2011 campaign (top panel) and the measured H_2O_{FISH} and the interpolated H_2O_{ERA} and H_2O_{ANA} along the flight track (bottom panel). The flight took place on 1 April 2011 over the US between 15–40° N with a two-times crossing of the subtropical jet stream in the vicinity of the thermal tropopause. Measurements are both in the troposphere and stratosphere. Positive deviations of the ECMWF water vapor mixing ratio appear both at the beginning and at the end of the flight when the aircraft ascended and descended through the troposphere. A fairly good agreement is observed in regions where the airplane samples stratospheric air masses, e.g., from 18:00–18:30 UTC and from 21:00–21:30 UTC, and in the vicinity of the thermal tropopause at around 16 to 18 km on the poleward side of the subtropical jet stream. Largest deviations appear in air masses of the middle tropical troposphere at around 12 km, e.g., at 20:00 UTC, when the ECMWF underestimates the observed water vapor content. There are also regions with a significant overestimation of the observed water vapor on the equatorward side of the subtropical jet stream, a region influenced by frequent two-way exchange across the jet stream connected with mixing of tropospheric and stratospheric air masses. When comparing H_2O_{ERA} and H_2O_{ANA} in more detail the measurements are better represented by H_2O_{ANA} than by H_2O_{ERA} in the deeper troposphere and close to the jet stream roughly between 19:15–20:45 UTC. This may well be explained by an improvement of the ECMWF data

ACPD
14, 14399–14438, 2014

assimilation system over four years. H_2O_{ERA} is based on the IFS release Cy31r2 in 2007 and H_2O_{ANA} on Cy36r1 in 2011. However, there are regions in the stratosphere with water vapor mixing ratios lower than 5 ppmv where H_2O_{ERA} slightly better represents H_2O_{FISH} than H_2O_{ANA}. During ascent and descent H_2O_{ERA} and H_2O_{ANA} agree fairly well.

For a quantification of these deviations in water vapor mixing ratio between the ECMWF and FISH the ratio $\Delta(H_2O)$ both for H_2O_{ANA} and H_2O_{ERA} is shown in Fig. 3 (left panel). For this example flight both $\Delta(H_2O_{ANA})$ and $\Delta(H_2O_{ERA})$ vary between 0.5 and 2, i.e., there are regions where the ECMWF under- but also overestimates the measurements up to a factor of two. Around 70 % of the values are close to $\Delta(H_2O) = 1$ and thus represent a nearly perfect relationship. The ascent and descent, and the parts in the vicinity of the equatorward side of the subtropical jet stream clearly show an enhanced $\Delta(H_2O)$ up to 2. These are the regions where H_2O_{ANA} agrees better with H_2O_{FISH} than H_2O_{ERA}. In the stratosphere there is a good agreement with $\Delta(H_2O) \approx 1$. The mean water vapor mixing ratio per $\Delta(H_2O)$ bin confirms that H_2O_{ANA} better represents H_2O_{FISH} than H_2O_{ERA} in this case study (Fig. 3, right panel).

The influence of the FISH measurement uncertainty on the ratio $\Delta(H_2O)$ is lower than 10 %. According to Sect. 2.1.1 we assume an instrument accuracy of 6 % for H_2O_{FISH} = 4 ppmv and of 8 % for H_2O_{FISH} = 100 ppmv. An overestimation of these water vapor mixing ratios of $\Delta(H_2O) = 2$ is therefore connected with an uncertainly range between 1.89 and 2.13 for $H_2O_{FISH} = 4 \pm 0.24$ ppmv and with an uncertainty range between 1.85 and 2.17 for $H_2O_{FISH} = 100 \pm 8$ ppmv.

3 Water vapor evaluation: ERA-Interim vs. FISH

Taking all measurements together, around 30 % of the data are very well represented by the model with $\Delta(H_2O_{ERA}) = 0.9–1.1$. The majority of the data, i.e., 57 %, are within the $\Delta(H_2O_{ERA})$ bins 0.5–0.9 and 1.1–2.0, and 13 % are connected with a strong under- ($\Delta(H_2O_{ERA}) < 0.5$) or overestimation ($\Delta(H_2O_{ERA}) > 2$). Over- and underestimations are

ACPD
14, 14399–14438, 2014

found both in the stratosphere and troposphere, whereas the troposphere is characterized by larger deviations than the stratosphere, as discussed in more detail in following sections.

3.1 Campaign-based analysis

Since the measurement campaigns represent different geographical and altitude regions (see Fig. 1) the comparison between ERA-Interim and FISH water vapor is first performed for each campaign separately.

Figure 4 (left panels, respectively) shows the frequency distribution of $\Delta(H_2O_{ERA})$ for each campaign. The range of $\Delta(H_2O_{ERA})$ is between 0.1 and 10.0 and its bin size is variable to represent reasonable scales. $\Delta(H_2O_{ERA})$ values between 1/7 and 5 are found, i.e., the model occasionally underestimates the observations up to a factor 7 and overestimates them up to a factor 5. Dependent on the campaign, around 10–20 % of the data are within a $\Delta(H_2O_{ERA})$ range between 0.9 and 1.1 indicating an almost perfect agreement between the reanalyses and observations. The majority of the data, i.e., around 40–80 %, are within the $\Delta(H_2O)$ ranges of 0.5–0.9 and 1.1–2 indicating a fairly good agreement. This is also confirmed by the mean and median values of $\Delta(H_2O)$, which are close to each other for all campaigns. The range of the mean of $\Delta(H_2O_{ERA})$ is from 1.03 (AMMA2006) to 1.41 (POLARCAT2008). In contrast, the variance of the data around the mean is different between the campaigns. The standard deviation of $\Delta(H_2O_{ERA})$ ranges from 0.19 (RECONCILE2010) to 0.82 (POLARCAT2008). Especially the SPURT campaigns, which contain data from different seasons and atmospheric situations have a larger variance around the mean than campaigns like RECONCILE2010 which include data from one single season and a polar vortex oriented flight strategy (von Hobe et al., 2013).

Figure 4 (right panels, respectively) also shows the mean H_2O_{ERA} and H_2O_{FISH} per $\Delta(H_2O_{ERA})$ bin. The mean mixing ratios corresponding to $\Delta(H_2O_{ERA}) = 0.9–1.1$ range from 7 ppmv (e.g., SCOUT2005, ENVISAT2002–2003, EUPLEX2003, and RECONCILE2010) to 300 ppmv (e.g., POLARCAT2008). This indicates that ERA-Interim

ACPD
14, 14399–14438, 2014

shows accurate water vapor values for both very dry and much moister conditions. There are campaigns, e.g., TROCCINOX2005, where ERA-Interim significantly underestimates the measurements at water vapor mixing ratios larger than 50 ppmv, and overestimates the measurements for mixing ratios lower than 50 ppmv. A similar relation for different water vapor values is shown for AMMA2006 also in the tropics and RECONCILE2010 in polar regions. Other campaigns, e.g., ENVISAT2002–2003 and EUPLEX2003, do not show this relationship and ERA-Interim over- and underestimates measurements larger than 50 ppmv.

In summary, a fairly good agreement of mixing ratios with $\Delta(H_2O_{ERA}) \approx 1$ occurs both at low mixing ratios (H_2O <10 ppmv) but also at high mixing ratios (H_2O > 300 ppmv). Based on this evaluation of individual measurement campaigns there is generally an increasing underestimation towards higher values of the FISH. To gain insight into the regions of the UTLS where over- and underestimations occur, the data of all campaigns is now analyzed with regard to the location relative to the position of the tropopause and upper-tropospheric jet streams.

3.2 Tropopause-based analysis in three atmospheric domains

Following Kunz et al. (2013) the measurement locations are divided into three atmospheric domains with respect to the height of the thermal tropopause (TP_H). In the climatological mean, the tropics are characterized by a thermal tropopause height above 14 km, whereas in the extratropics tropopause heights are usually lower than 12 km. The tropical and the extratropical domain are separated by the subtropical jet stream characterized by an intermediate tropopause height. The FISH-based climatology is therefore analyzed with respect to the three atmospheric domains:

- Tropical measurements (TROP): TP_H >14 km
- Subtropical measurements (SUBTROP): 12 km ≤ TP_H ≤ 14 km
- Extratropical measurements (EXTROP): TP_H <12 km

ACPD
14, 14399–14438, 2014

The separation of the FISH-based water vapor climatology according to these three domains attributes 26 % of data to the tropical, 17 % to the subtropical, and 57 % to the extratropical domain. However, the proposed selection allows a detailed look at $\Delta(H_2O_{ERA})$ for tropical and extratropical measurement locations without mixing dynamical processes on the equatorward and poleward side of the subtropical jet stream (see Fig. 1, bottom panel). In addition, subtropical measurements under a more frequent influence of the subtropical jet stream are separately considered.

Figure 5 (top row) shows $\Delta(H_2O_{ERA})$ and the counts of measurements for the three atmospheric domains with respect to the distance from the thermal tropopause. The counts are calculated for 1 km thick layers and the $\Delta(H_2O_{ERA})$ bins are organized as for Fig. 4. Measurements have been made between –10 to 5 km around the tropopause in the tropical domain and between –6 to 10 km in the extratropical domain. Clear measurement frequency maxima are in the vicinity of the tropopause in the tropical domain, and again at the tropopause and also 6 to 9 km above the tropopause in the extratropical domain. The subtropical domain is characterized by a relatively uniform vertical distribution of measurements with no pronounced maximum between –6 to 6 km relative to the tropopause. These distributions show the representativeness of individual tropopause and $\Delta(H_2O_{ERA})$ bins and should be kept in mind when analyzing the key results.

For all three atmospheric domains, near the measurement frequency peaks the values of $\Delta(H_2O_{ERA})$ are between 0.5 and 2. ERA-Interim more strongly over- and underestimates the FISH measurements in the troposphere for the tropical and extratropical domains and in the lower stratosphere for the extratropical domain. Here, $\Delta(H_2O_{ERA})$ may reach values larger than 4 and lower than 0.25. In the tropical domain, the range of $\Delta(H_2O_{ERA})$ is lower in the stratosphere than in the troposphere which is not observed in the other atmospheric domains, where values of $\Delta(H_2O_{ERA})$ between 0.1 and 10 occur for bins with low counts of measurements. At the thermal tropopause, the range of $\Delta(H_2O_{ERA})$ increases from the tropics toward the extratropics with $\Delta(H_2O_{ERA})$ from 0.5 to 2 in the tropical domain, and from 0.33 to 4 in the extratropical domain.

ACPD
14, 14399–14438, 2014

Strong underestimations, i.e., $\Delta(H_2O_{ERA}) < 0.5$, in the troposphere on isentropes below 330 K are connected with a FISH water vapor mixing ratio > 400 ppmv (Fig. 5, middle and bottom rows). An overestimation in the upper troposphere is observed for mixing ratios < 400 ppmv both in the tropics and extratropics. Very low FISH water vapor mixing ratios < 10 ppmv in the lower stratosphere lower than 3 km above the tropopause are overestimated by a factor up to 2 in the tropics and up to 4 in the extratropics. On higher levels in the stratosphere connected with isentropic layers above 370 K these low FISH measurements are strongly underestimated by a factor up to 3.

Over- and underestimations are found both in the troposphere and in the stratosphere. In the tropics the spread of $\Delta(H_2O_{ERA})$ increases with increasing water vapor mixing ratio from the stratosphere toward the troposphere. This is also reflected by the correlation between ERA-Interim and FISH water vapor mixing ratio (Fig. 6, top panel), which shows that the correlation between ERA-Interim and FISH mixing ratios gets weaker toward higher mixing ratios. This relationship is weaker in the extratropical domain (Fig. 6, bottom panel).

3.3 Equivalent latitude-based analysis on isentropes

The potential temperature and equivalent latitude coordinates provide an isentropic view on the relation between H_2O_{ERA} and H_2O_{FISH} (Fig. 7). Here, the isentropic concept of equivalent latitude is used to reduce the effects of reversible transport processes in the UTLS (Olsen et al., 2010; Pan et al., 2012). At the same time, the location of the dynamic tropopause based on the maximum isentropic PV-gradient is determined according to Kunz et al. (2011a). This PV-gradient based tropopause is in the vicinity of the core of the subtropical jet stream on isentropes between 320 to 380 K (Fig. 7, top panel). Figure 8 therefore represents the quasi-horizontal distance of the FISH measurements in equivalent latitude from the PV gradient-based tropopause on isentropes between 300 and 380 K with negative values representing measurements on the equatorward side of the jet stream and vice versa (see also Kunz et al., 2011b; Pan et al., 2012). The location of the jet stream is characterized by the highest frequency of FISH

ACPD
14, 14399–14438, 2014

measurements (Fig. 7, top panel). This area of high sampling frequency extends up to 20° around the jet stream core and is related to a $\Delta(H_2O_{ERA})$ between 0.5 and 2 (Fig. 8, top panel).

In general, there is an overestimation of water vapor by ERA-Interim with $\Delta(H_2O_{ERA})$ between 1.1 and 2 on all isentropes between 300 and 380 K both poleward of the subtropical jet stream in the lower stratosphere and equatorward in the upper troposphere (Fig. 7, middle panel and Fig. 8, middle panel). In the vicinity of the jet stream on isentropes around the jet core, i.e., on 360 K and between 320 and 340 K, there are two pronounced areas where the model represents the observations very well according to a $\Delta(H_2O_{ERA})$ between 0.9 and 1.1 (Fig. 7, middle panel). In the lower stratosphere on isentropes between 360 and 380 K and in the lower troposphere below 310 K, ERA-Interim overestimates the observations up to a factor of two. Pronounced maxima of $\Delta(H_2O_{ERA}) > 2$ are found in the tropical troposphere on 350 K at an equivalent latitude lower than 20°, in the extratropical lower stratosphere on 340 K at an equivalent latitude higher than 80°, and on low isentropes around 300 K at midlatitudes. The regions of these maxima reflect the areas with strong overestimations of water vapor shown relatively to the thermal tropopause in Fig. 5.

There is a pronounced maximum of the mean H_2O_{FISH} mixing ratio in the vicinity of the dynamic tropopause on isentropes between 300 and 320 K (Fig. 7, bottom panel). In this area $\Delta(H_2O_{ERA})$ is close to two. On the same isentropes there are regions with a high mean H_2O_{FISH} mixing ratio that are both overestimated and underestimated by the model around 30° equivalent latitude equatorward of the dynamic tropopause (Fig. 8, bottom panel). In regions with an underestimation the mean water vapor mixing ratio is higher (> 200 ppmv) than in regions with overestimation. In contrast, water vapor mixing ratios of lower than 10 ppmv in the stratosphere poleward of the subtropical jet stream are largely overestimated by ERA-Interim most of the times.

In summary, both over- and underestimations are found in the troposphere and stratosphere both poleward and equatorward of the subtropical jet stream. Near the core of the subtropical jet stream around 350 K, values of $\Delta(H_2O_{ERA})$ are between 1.1

ACPD
14, 14399–14438, 2014

and 2.0 whereas the isentropes above and below are connected with an almost perfect relationship of $\Delta(H_2O_{ERA})$ between 0.9 and 1.1. According to Figs. 7 and 8, the largest problems occur toward the tropics and the polar regions between 340 and 360 K, in agreement with the previous results.

4 Water vapor evaluation: operational analyses vs. FISH

By using the FISH-based water vapor climatology the temporal development of the quality of the ECMWF operational analyses in terms of water vapor in the UTLS is addressed separately for measurements in the stratosphere above the thermal tropopause (Fig. 9) and in the troposphere below the thermal tropopause (Fig. 10). The analysis is made separately for the different IFS Cycles during the eleven years from 2001 to 2011. Therefore, the daily mean ratio between the operational analysis and FISH water vapor, $\Delta(H_2O_{ANA})$, and the range between the maximum and minimum value are presented for each single measurement day. For comparison, the daily mean $\Delta(H_2O_{ERA})$ is also discussed, which represents the IFS Cycle 31r2, taken for operational forecasting from 12 December 2006 until 5 June 2007.

Over the entire period between 2001 and 2011 the daily mean $\Delta(H_2O_{ANA})$ varies between 0.5 and 2 within the tropical stratosphere (Fig. 9, top left panel). Toward the extratropical stratosphere the daily mean $\Delta(H_2O_{ANA})$ varies stronger (Fig. 9, bottom left panel). In particular, from 2001 to the end of 2003 the daily mean $\Delta(H_2O_{ANA})$ varies between 0.25 and 2, i.e., the model more strongly underestimates than overestimates most of the measurements. During this time period, observations are mainly from the SPURT campaign in different seasons. Comparing the daily mean $\Delta(H_2O_{ANA})$ between the time periods before 2004 and after 2009 shows that $\Delta(H_2O_{ANA})$ yields a value of $\Delta(H_2O) \approx 1$ more often in the later period, in particular in the tropical stratosphere.

Figure 9 (right panels) shows the correlation of H_2O_{FISH} with H_2O_{ANA} and with H_2O_{ERA} for two selected time periods with IFS Cycles 28r1–31r1 (9 March 2004 to 12 September 2006) and IFS Cycles 36r1–37r2 (26 January 2010 to 18 May 2011).

ACPD
14, 14399–14438, 2014

It should be noted that the updates within these selected periods may influence the related correlation between the measurements and the model. There is the tendency that strong overestimations with $\Delta(H_2O_{ANA}) > 2$ are related with H_2O_{FISH} of lower than 5 ppmv. This is observed for IFS Cycles 28r1–31r1 and 36r1–37r2 (e.g., Fig. 9 middle panels) indicating that those problems of overestimations of low mixing ratios remain for both IFS Cycles. In contrast, underestimations with a $\Delta(H_2O_{ANA}) < 0.5$ are observed for measurements higher than 20 ppmv. These strong deviations from the measurements are found in the subtropical and extratropical stratosphere for the second period of IFS Cycles 36r1–37r2 (Fig. 9 middle and bottom right panels). In the subtropical stratosphere, these strong overestimations are reduced with a better H_2O_{ANA} than H_2O_{ERA} for the second period of IFS Cycles 36r1–37r2 (Fig. 9 middle right panel). This may well show the improvement of the later model cycle compared to the model cycle used for ERA-Interim, as also shown in Figs. 2 and 3.

In the troposphere (Fig. 10), there is also strong variability of the daily mean $\Delta(H_2O_{ANA})$ from 2001 to 2011 both in the tropics and the extratropics. In the first years after 2007 the range of $\Delta(H_2O_{ANA})$ in the extratropical troposphere increases despite a change of the assimilation scheme of IFS Cycle 31r1 allowing full supersaturation with respect to ice that also has an influence on upper tropospheric humidity which consequently increased in the analysis data (Tompkins et al., 2007). The increase of $\Delta(H_2O_{ANA})$ after 2007 is weaker in the extratropical stratosphere (Fig. 9, bottom panel). This may be influenced by the fact that humidity data is not assimilated above the tropopause. Anyhow, other changes of data assimilation and model resolution may contribute to the observed increase of $\Delta(H_2O_{ANA})$ in the extratropical troposphere after 2007.

When comparing $\Delta(H_2O_{ANA})$ between the stratosphere and the troposphere for single years, e.g., 2006, there is the tendency that the tropical troposphere is characterized by a larger variance of $\Delta(H_2O_{ANA})$ than the tropical stratosphere. In contrast, the extratropical troposphere is characterized by a lower variance of $\Delta(H_2O_{ANA})$ than the extratropical stratosphere, in particular for the period before 2004. This may well show

ACPD
14, 14399–14438, 2014

the difficulty to accurately simulate the influence of tropical tropospheric processes as well as extratropical stratospheric processes on the water vapor distribution. Similar to the stratosphere (Fig. 9), the correlation of H_2O_{FISH} and H_2O_{ANA} in the troposphere shows the tendency of the model to overestimate low and underestimate high mixing ratios. There is no clear difference between ERA-Interim and operational analyses, indicating that these problems remain irrespective of the data assimilation cycle and model resolution.

5 Summary and discussion

The latest reanalysis product by the ECMWF, the ERA-Interim data set, is evaluated using the global FISH-based water vapor climatology. This climatology represents a valuable data set of high-quality airborne water vapor measurements performed during ten aircraft campaigns from 2001 to 2011 (see Table 1). The advantage of the FISH-based water vapor climatology is that water vapor is measured with a high accuracy throughout the UTLS, a region where satellite data have difficulties to accurately measure trace gas distributions. In addition, all water vapor measurements used for this analysis are based on the same measurement technique. Thus, this data set proves to be well suited for a model evaluation since the results are not influenced by changing measurement accuracies that may arise due to different water vapor instruments at different aircraft campaigns (Tilmes et al., 2010) or due to a height dependent sensitivity of the measurement instrument (Kunz et al., 2008).

The analysis in this study extends short-term evaluations of ECMWF water vapor analyses over Brazil and Europe in 2004 and 2007 (Flentje et al., 2007; Schäfler et al., 2010). At the same time, the improvement of the representation of UTLS water vapor in different operational analysis cycles of the IFS is considered. The FISH-based water vapor climatology allows a detailed evaluation of simulated water vapor fields separately for tropical and extratropical regions. These regions are determined according to

ACPD
14, 14399–14438, 2014

their characteristic thermal tropopause heights, i.e., larger than 14 km and lower than 12 km, following the approach of Kunz et al. (2013).

There is generally a good agreement between ERA-Interim and FISH water vapor values, i.e., H_2O_{FISH} and H_2O_{ERA}. The ratio $\Delta(H_2O_{ERA})$ is between 0.5 and 2 for more than 87 % of all observations. About 30 % of these measurements are nearly perfectly represented by the model with $\Delta(H_2O_{ERA}) = 1.0 \pm 0.1$. In some cases, ERA-Interim significantly over- and underestimates the FISH measurements. For 13 % of the data $\Delta(H_2O_{ERA})$ is either lower than 0.5 or larger than 2. In the troposphere, these severe under- and overestimations are observed in the tropics and extratropics. In the lower stratosphere, ERA-Interim well reflects the observations in the tropics, whereas in the extratropics large over- and underestimations occur, with $\Delta(H_2O_{ERA})$ values larger than 4 and lower than 0.25. In general, the range of $\Delta(H_2O_{ERA})$ is lower in the stratosphere than in the troposphere.

Similar to ERA-Interim the operational analyses have the tendency to overestimate low mixing ratios and underestimate high mixing ratios. A case study of H_2O_{ANA} for a particular MACPEX flight in 2011 shows that the overestimation of water vapor near the flanks of the subtropical jet stream is reduced by a factor of two compared with H_2O_{ERA} (Fig. 3). Further, in the subtropical lower stratosphere the underestimation of water vapor is stronger for H_2O_{ERA} than for H_2O_{ANA}. This may well reflect the improvement of the model cycle used in 2011 that benefits from several relevant changes compared to the model cycle used in 2007.

The evaluation of H_2O_{ERA} and H_2O_{ANA} indicates that the influence of tropospheric processes on the water vapor mixing ratio is particularly challenging for the assimilation system. These processes include deep convection, cloud microphysics and transport. Additionally, extratropical dynamical processes like mixing, cross-tropopause exchange and convective injections into the lower stratosphere (e.g., Schiller et al., 2009; Ravishankara, 2012; Ploeger et al., 2013) may affect the quality of ECMWF (re)analyses water vapor in the extratropical lower stratosphere. Dyroff et al. (2014) indicated an insufficient model resolution of small scale intrusions of air masses in the UTLS and

ACPD
14, 14399–14438, 2014

an influence of numerical diffusion associated with the advection scheme in the vicinity of sharp humidity gradients at the tropopause. These issues may be possible contributors to the model bias in the lower stratosphere (see also Stenke et al., 2008). In our study, the tropical troposphere and the extratropical UTLS turn out as atmospheric regions with challenging dynamics where both ERA-Interim and the operational analyses may significantly deviate from the observations. This evaluation indicates no clear difference between ERA-Interim and operational analyses. Problems therefore remain concerning the data assimilation cycle and model resolution to accurately simulate the influence of tropospheric processes as well as extratropical stratospheric processes on the water vapor distribution.

The results of this study might be biased because of the different flight strategies of the campaigns included in the FISH-based water vapor climatology. However, this study represents a comprehensive overview of the ECMWF water vapor distribution in the UTLS from the tropics toward the poles and a validation with independent observations. The results of this study are therefore particularly relevant for studies of the UTLS using ERA-Interim water vapor fields. These data have been frequently used for climatologies and trend studies over the past 30 years. Furthermore, the assessment of operational analysis water vapor is valuable for their possible use in the numerical modeling of ice clouds. The correct simulation of the onset of ice nucleation and the prediction of ice clouds in the upper troposphere, e.g., based on coupled versions of Lagrangian and microphysical models, are particularly dependent on the quality of the input water vapor fields.

Acknowledgements. This analysis has been performed in memory of C. Schiller facilitating the "FISH-based water vapor climatology" as developer and PI of the FISH instrument during his life's work. A. Kunz has been supported by the European Union Seventh Framework Programme (FP7/2007–2013) under grant agreement no. 299666 with the Marie Curie Fellowship "Dynamical processes in the tropopause region and their impact on the distribution of atmospheric trace gases" (PROTRO). Many thanks to the ECMWF for providing their products. We are also grateful to J.-U. Grooß , M. Krämer and P. Spichtinger for helpful discussions.

ACPD
14, 14399–14438, 2014

References

Blom, C. E., Cortesi, U., and Redaelli, G.: ENVISAT validation: introduction to the correlative measurements by the chemistry payload on board the M–55 Geophysica, Proc. of the 16th ESA Symposium on European Rocket and Balloon Programmes and Related Research, St. Gallen, Switzerland, 1–6, 2–5 June 2003 (ESA SP-530, August 2003). 14427

Cairo, F., Pommereau, J. P., Law, K. S., Schlager, H., Garnier, A., Fierli, F., Ern, M., Streibel, M., Arabas, S., Borrmann, S., Berthelier, J. J., Blom, C., Christensen, T., D'Amato, F., Di Donfrancesco, G., Deshler, T., Diedhiou, A., Durry, G., Engelsen, O., Goutail, F., Harris, N. R. P., Kerstel, E. R. T., Khaykin, S., Konopka, P., Kylling, A., Larsen, N., Lebel, T., Liu, X., MacKenzie, A. R., Nielsen, J., Oulanowski, A., Parker, D. J., Pelon, J., Polcher, J., Pyle, J. A., Ravegnani, F., Rivière, E. D., Robinson, A. D., Röckmann, T., Schiller, C., Simões, F., Stefanutti, L., Stroh, F., Some, L., Siegmund, P., Sitnikov, N., Vernier, J. P., Volk, C. M., Voigt, C., von Hobe, M., Viciani, S., and Yushkov, V.: An introduction to the SCOUT-AMMA stratospheric aircraft, balloons and sondes campaign in West Africa, August 2006: rationale and roadmap, Atmos. Chem. Phys., 10, 2237–2256, doi:10.5194/acp-10-2237-2010, 2010. 14427

Castanheira, J. M., Peevey, T. R., Marques, C. A. F., and Olsen, M. A.: Relationships between Brewer–Dobson circulation, double tropopauses, ozone and stratospheric water vapour, Atmos. Chem. Phys., 12, 10195–10208, doi:10.5194/acp-12-10195-2012, 2012. 14402

Dee, D. P., Uppala, S. M., Simmons, A. J., Berrisford, P., Poli, P., Kobayashi, S., Andrea, U., Balmaseda, M. A., Balsamo, G., Bauer, P., Bechthold, P., Beljaars, A. C. M., von de Berg, L., Bidlot, J., Bormann, N., Delsol, C., Dragani, R., Fuentes, M., Geer, A. J., Haimberger, L., Healy, S. B., Hersbach, H., Hólm, E. V., Isaksen, L., Kallberg, P., Köhler, M., Matricardi, M., McNally, A. P., Monge-Sanz, B. M., Morcrette, J.-J., Park, B.-K., Peubey, C., de Rosnay, P., Tavolato, C., Thépaut, J.-N., and Vitart, F.: The ERA-Interim reanalysis: configuration and performance of the data assimilation system, Q. J. Roy. Meteor. Soc., 137, 553–597, doi:10.1002/qj.828, 2011. 14401, 14406, 14407

Dyroff, C., Zahn, A., Christner, E., Forbes, R. M., Tompkins, A. M., and van Velthoven, P. F. J.: Comparison of ECMWF analysis and forecast humidity data to CARIBIC upper troposphere and lower stratosphere observations, Q. J. Roy. Meteor. Soc., doi:10.1002/qj.2400, 2014. 14403, 14419

ACPD
14, 14399–14438, 2014

Engel, A., Bönisch, H., Brunner, D., Fischer, H., Franke, H., Günther, G., Gurk, C., Hegglin, M., Hoor, P., Königstedt, R., Krebsbach, M., Maser, R., Parchatka, U., Peter, T., Schell, D., Schiller, C., Schmidt, U., Spelten, N., Szabo, T., Weers, U., Wernli, H., Wetter, T., and Wirth, V.: Highly resolved observations of trace gases in the lowermost stratosphere and upper troposphere from the Spurt project: an overview, Atmos. Chem. Phys., 6, 283–301, doi:10.5194/acp-6-283-2006, 2006. 14404, 14427

Flentje, H., Dörnbrack, A., Fix, A., Ehret, G., and Hólm, E.: Evaluation of ECMWF water vapour fields by airborne differential absorption lidar measurements: a case study between Brazil and Europe, Atmos. Chem. Phys., 7, 5033–5042, doi:10.5194/acp-7-5033-2007, 2007. 14401, 14402, 14404, 14418

Forster, P. M. de F., and Shine, K. P.: Radiative forcing and temperature trends from stratospheric ozone changes, J. Geophys. Res., 102, 10841–10855, 1997. 14401

Fueglistaler, S., Dessler, A. E., Dunkerton, T. J., Folkins, I., Fu, Q., and Mote, P. W., Tropical tropopause layer, Rev. Geophys., 47, RG1004, doi:10.1029/2008RG000267, 2009. 14401

Haynes, P. and Shuckburgh, E.: Effective diffusivity as a diagnostic of atmospheric transport 2. Troposphere and lower stratosphere, J. Geophys. Res., 105, 22795–22810, 2000. 14401

Jensen, E. and Pfister, L.: Transport and freeze-drying in the tropical tropopause layer, J. Geophys. Res., 109, D02207, doi:10.1029/2003JD004022, 2004. 14401

Jones, R. L. and Pyle, J. A.: Observations of CH_4 and N_2O by the NIMBUS 7 SAMS: a comparison with in situ data and two-dimensional numerical model calculations, J. Geophys. Res., 89, 3D1644, doi:10.1029/JD089iD04p05263, 1984. 14401

Köhler, M., Ahlgrimm, M., and Beljaars, A. C. M.: Unified treatment of dry convective and stratocumulus-topped boundary layers in the ECMWF model, Q. J. Roy. Meteor. Soc., 137, 43–57, 2011. 14407

Kunz, A., Schiller, C., Rohrer, F., Smit, H. G. J., Nedelec, P., and Spelten, N.: Statistical analysis of water vapour and ozone in the UT/LS observed during SPURT and MOZAIC, Atmos. Chem. Phys., 8, 6603–6615, doi:10.5194/acp-8-6603-2008, 2008. 14403, 14405, 14418

Kunz, A., Konopka, P., Müller, R., and Pan, L. L.: Dynamical tropopause based on isentropic potential vorticity gradients, J. Geophys. Res., 116, D01110, doi:10.1029/2010JD014343, 2011a. 14408, 14414

Kunz, A., Pan, L. L., Konopka, P., Kinnison, D. E., and Tilmes, S.: Chemical and dynamical discontinuity at the extra-tropical tropopause-based on START08 and WACCM analyses, J. Geophys. Res., 116, D24302, doi:10.1029/2011JD016686, 2011b. 14401, 14408, 14414

ACPD
14, 14399–14438, 2014

Kunz, A., Müller, R., Homonnai, V., Jánosi, I. M., Hurst, D., Rap, A., Forster, P. M., Rohrer, F., Spelten, N., and Riese, M.: Extending water vapor trend observations over Boulder into the tropopause region: trend uncertainties and resulting radiative forcing, J. Geophys. Res., 118, 11269–11284, doi:10.1002/jgrd.50831, 2013. 14412, 14419

Luo, Z., Kley, D., Johnson, R. H., and Smit, H.: Ten years of measurements of tropical upper-tropospheric water vapor by MOZAIC, Part II: Assessing the ECMWF humidity analysis, J. Climate, 21, 1449–1466, doi:10.1175/2007JCLI1887.1, 2007. 14403

McKenna, D. S., Konopka, P., Grooß, J.-U., Günther, G., Müller, R., Spang, R., Offermann, D., and Orsolini, Y.: A new Chemical Lagrangian Model of the Stratosphere (CLaMS): 1. Formulation of advection and mixing, J. Geophys. Res., 107, 4309, doi:10.1029/2000JD000114, 2002. 14407

Oikonomou, E. K. and O'Neill, A.: Evaluation of ozone and water vapor fields from the ECMWF reanalysis ERA-40 during 1991–1999 in comparison with UARS satellite and MOZAIC aircraft observations, J. Geophys. Res., 111, D14109, doi:10.1029/2004JD005341, 2006. 14403

Olsen, M. A., Douglas, A. R., Schoeberl, M. R., Rodriguez, J. M., and Yoshida, Y.: Interannual variability of ozone in the winter lower stratosphere and the relationship to lamina and irreversible transport, J. Geophys. Res., 115, D15305, doi:10.1029/2009JD013004, 2010. 14414

Pan, L. L., Randel, W. J., Gary, B. L., Mahoney, M. J., and Hintsa, E. J.: Definition and sharpness of the extratropical tropopause: a trace gas perspective, J. Geophys. Res., 109, D23103, doi:10.1029/2004JD004982, 2004. 14401

Pan, L. L., Kunz, A., Homeyer, C. R., Munchak, L. A., Kinnison, D. E., and Tilmes, S.: Commentary on using equivalent latitude in the upper troposphere and lower stratosphere, Atmos. Chem. Phys., 12, 9187–9199, doi:10.5194/acp-12-9187-2012, 2012. 14414

Ploeger, F., Günther, G., Konopka, P., Fueglistaler, S., Müller, R., Hoppe, C., Kunz, A., Spang, R., Grooß, J.-U., and Riese, M.: Horizontal water vapor transport in the lower stratosphere from subtropics to high latitudes during boreal summer, J. Geophys. Res., 118, 1–17, doi:10.1002/jgrd.50636, 2013. 14402, 14407, 14419

Ravishankara, A. R.: Water vapor in the lower stratosphere, Science, 337, 809–810, 2012. 14419

ACPD
14, 14399–14438, 2014

Riese, M., Ploeger, F., Rap, A., Vogel, B., Konopka, P., Dameris, M., and Forster, P.: Impact of uncertainties in atmospheric mixing on simulated UTLS composition and related radiative effects, J. Geophys. Res., 117, D16305, doi:10.1029/2012JD017751, 2012. 14401

Röckmann, T., Grooß, J.-U., and Müller, R.: The impact of anthropogenic chlorine emissions, stratospheric ozone change and chemical feedbacks on stratospheric water, Atmos. Chem. Phys., 4, 693–699, doi:10.5194/acp-4-693-2004, 2004. 14401

Rohrer, F. and Berresheim, H.: Strong correlation between levels of tropospheric hydroxyl radicals and solar ultraviolet radiation, Nature, 442, 184–187, 2006. 14401

Rohs, S., Schiller, C., Riese, M., Engel, A., Schmidt, U., Wetter, T., Levin, I., Nakazawa, T., and Aoki, S.: Long-term changes of methane and hydrogen in the stratosphere in the period 1978–2003 and their impact on the abundance of stratospheric water vapor, J. Geophys. Res., 111, doi:10.1029/2005JD006877, D14315, 2006. 14401

Schäfler, A., Dörnbrack, A., Kiemle, C., Rahm, S., and Wirth, M.: Tropospheric water vapor transport as determined from airborne lidar measurements, J. Atmos. Ocean. Techn., 27, 2017–2030, doi:10.1175/2010JTECHA1418.1, 2010. 14402, 14418

Schiller, C., Grooß, J.-U., Konopka, P., Plöger, F., Silva dos Santos, F. H., and Spelten, N.: Hydration and dehydration at the tropical tropopause, Atmos. Chem. Phys., 9, 9647–9660, doi:10.5194/acp-9-9647-2009, 2009. 14401, 14404, 14419

Solomon, S., Rosenlof, K. H., Portman, R. W., Daniel, J. S., Davis, S. M., Sanford, F. J., and Plattner, G.-K.: Contributions of stratospheric water vapor to decadal changes in the rate of global warming, Science, 327, 1219–1223, 2010. 14401

Stenke, A., Grewe, V., and Ponater, M.: Lagrangian transport of water vapor and cloud water in the ECHAM4 GCM and its impact on the cold bias, Clim. Dynam., 31, 491–506, 2008. 14403, 14420

Tilmes, S., Pan, L. L., Hoor, P., Atlas, E., Avery, M. A., Campos, T., Christensen, L. E., Diskin, G. S., Gao, R.-S., Herman, R. L., Hintsa, E. J., Loewenstein, M., Lopez, J., Paige, M. E., Pittman, J. V., Podolske, J. R., Proffitt, M. R., Sachse, G. W., Schiller, C., Schlager, H., Smith, J., Spelten, N., Webster, C., Weinheimer, A., and Zondlo, M. A.: An aircraft-based upper troposphere lower stratosphere O_3, CO, and H_2O climatology for the Northern Hemisphere, J. Geophys. Res., 115, D14303, doi:10.1029/2009JD012731, 2010. 14406, 14418

Tompkins, A. M., Gierens, K., and Rädel, G.: Ice supersaturation in the ECMWF integrated forecast system, Q. J. Roy. Meteor. Soc., 133, 53–63, doi:10.1002/qj.14, 2007. 14407, 14417

ACPD
14, 14399–14438, 2014

Uppala, S. M., Kållberg, P. W., Simmons, A. J., Andrae, U., Bechtold, V. Da Costa, Fiorino, M., Gibson, J. K., Haseler, J., Hernandez, A., Kelly, G. A., Li, X., Onogi, K., Saarinen, S., Sokka, N., Allan, R. P., Andersson, E., Arpe, K., Balmaseda, M. A., Beljaars, A. C. M., Berg, L. Van De, Bidlot, J., Bormann, N., Caires, S., Chevallier, F., Dethof, A., Dragosavac, M., Fisher, M., Fuentes, M., Hagemann, S., Hólm, E., Hoskins, B. J., Isaksen, L., Janssen, P. A. E. M., Jenne, R., McNally, A. P., Mahfouf, J.-F., Morcrette, J.-J., Rayner, N. A., Saunders, R. W., Simon, P., Sterl, A., Trenberth, K. E., Untch, A., Vasiljevic, D., Viterbo, P., and Woollen, J.: The ERA-40 reanalysis, Q. J. Roy. Meteor. Soc., 131, 612, 2961–3012, doi:10.1256/qj.04.176, 2006. 14402

Vaughan, G., Schiller, C., MacKenzie, A. R., Bower, K., Peter, T., Schlager, H., Harris, N. R. P., and May, P. T. E.: SCOUT–O3/ACTIVE high-altitude aircraft measurements around deep tropical convection, BAMS, 89, 647–662, doi:10.1175/BAMS-89-5-647, 2008. 14427

von Hobe, M., Bekki, S., Borrmann, S., Cairo, F., D'Amato, F., Di Donfrancesco, G., Dörnbrack, A., Ebersoldt, A., Ebert, M., Emde, C., Engel, I., Ern, M., Frey, W., Genco, S., Griessbach, S., Grooß, J.-U., Gulde, T., Günther, G., Hösen, E., Hoffmann, L., Homonnai, V., Hoyle, C. R., Isaksen, I. S. A., Jackson, D. R., Jánosi, I. M., Jones, R. L., Kandler, K., Kalicinsky, C., Keil, A., Khaykin, S. M., Khosrawi, F., Kivi, R., Kuttippurath, J., Laube, J. C., Lefèvre, F., Lehmann, R., Ludmann, S., Luo, B. P., Marchand, M., Meyer, J., Mitev, V., Molleker, S., Müller, R., Oelhaf, H., Olschewski, F., Orsolini, Y., Peter, T., Pfeilsticker, K., Piesch, C., Pitts, M. C., Poole, L. R., Pope, F. D., Ravegnani, F., Rex, M., Riese, M., Röckmann, T., Rognerud, B., Roiger, A., Rolf, C., Santee, M. L., Scheibe, M., Schiller, C., Schlager, H., Siciliani de Cumis, M., Sitnikov, N., Søvde, O. A., Spang, R., Spelten, N., Stordal, F., Sumińska-Ebersoldt, O., Ulanovski, A., Ungermann, J., Viciani, S., Volk, C. M., vom Scheidt, M., von der Gathen, P., Walker, K., Wegner, T., Weigel, R., Weinbruch, S., Wetzel, G., Wienhold, F. G., Wohltmann, I., Woiwode, W., Young, I. A. K., Yushkov, V., Zobrist, B., and Stroh, F.: Reconciliation of essential process parameters for an enhanced predictability of Arctic stratospheric ozone loss and its climate interactions (RECONCILE): activities and results, Atmos. Chem. Phys., 13, 9233–9268, doi:10.5194/acp-13-9233-2013, 2013. 14404, 14411, 14427

World Meteorological Organization (1957): Meteorology – a three-dimensional science, WMO Bull., 6, 134–138, 1957. 14408

Zöger, M., Afchine, A., Eicke, N., Gerhards, M.-T., Klein, E., McKenna, D. S., Mörschel, U., Schmidt, U., Tan, V., Tuitjer, F., Woyke, T., and Schiller, C.: Fast in-situ stratospheric

ACPD
14, 14399–14438, 2014

hygrometers: a new family of balloon-borne and airborne Lyman α photofragment fluorescence hygrometers, J. Geophys. Res., 104, 1807–1816, 1999. 14405

ACPD
14, 14399–14438, 2014

Table 1. Information on campaigns of the FISH-based water vapor climatology including both local and transfer flights. The number of missions refer to the flight missions used for this climatology, i.e., the total amount of flight missions per campaign may be higher. The approximate regional extent of the 148 flight missions is shown in Fig. 1.

Campaign	Time	Location	Flight missions	Flight hours	Campaign objectives
SPURT (Trace gas transport in the tropopause region) e.g. Engel et al. (2006)	Nov 2001, Jan 2002 May 2002, Aug 2002 Oct 2002, Feb 2003 Apr 2003, Jul 2003	Hohn (Germany)	34	≈ 147	UTLS trace gas climatology Atmospheric transport and seasonal variation of trace gases
EUPLEX (European Polar Stratospheric Cloud and Lee Wave Experiment)	Jan 2003, Feb 2003	Kiruna (Sweden)	7	≈ 40	Polar Stratospheric Clouds Ozon loss in polar vortex Chlorine activation De- and renitrification
POLARCAT GRACE (Greenland Aerosol and Chemistry Experiment)	Jul 2008	Kangerlussuaq (Greenland)	13	≈ 80	Boreal forest fire emissions into the UTLS Annual variation of trace gases and aerosols in the Arctic
RECONCILE (Reconciliation of essential process parameters for an enhanced predictability of arctic strat. ozone loss and its climate interactions) e.g. von Hobe et al. (2013)	Jan 2010, Feb 2010 Mar 2010	Kiruna (Sweden)	13	≈ 52	Polar vortex chemical reactions Catalytic CLOx/BrOx chemistry Chlorine activation on PSCs NAT nucleation mechanisms
ENVISAT e.g. Blom et al. (2003)	Jun 2002, Oct 2002 Mar 2003	Forli (Italy) and Kiruna (Sweden)	10 5	≈ 44 ≈ 20	Validation of ENVISAT chemistry instruments at midlatitudes ENVISAT validation in the Arctic
CIRRUS	Dec 2003, Nov 2004 Nov 2006	Hohn (Germany)	12	≈ 52	Cirrus formation mechanism and radiative effects Chemical and microphysical properties of cloud particles
MACPEX (Midlatitude Airborne Cirrus Properties Experiment)	Apr 2011	Houston (USA,TX)	15	≈ 100	Cirrus formation mechanism H_2O instrumental inter-comparison
TROCCINOX (Tropical Convection, Cirrus, and Nitrogen Oxides Experiment) www.pa.op.dlr.de/troccinox	Jan 2005, Feb 2005	Aracatuba (Brazil)	14	≈ 64	Impact of tropical convection on UTLS trace gases and particles Lightning produced NO_x in tropical thunderstorms
SCOUT (Stratospheric-Climate Links with Emphasis on the Upper Troposphere and Lower Stratosphere) e.g. Vaughan et al. (2008)	Nov 2005, Dec 2005	Darwin (Australia)	16	≈ 88	Deep tropical convection Composition of the Tropical Transition Layer Transport of trace gases into the tropical UTLS
AMMA (African Monsoon Multidisciplinary Analysis) e.g. Cairo et al. (2010)	Jul 2006, Aug 2006	Ouagadougou (Burkina Faso)	9	≈ 40	Intense mesoscale convection connected with African monsoon Large scale transport into the UTLS Lightning and NO_x production

ACPD
14, 14399–14438, 2014

Table 2. Six different time intervals from 2001 to 2011 and their temporal limits for segregating the operational analysis water vapor fields regarding different ECMWF IFS model cycles.

Interval	Time	IFS Cycles
1.	Jun 2001–Mar 2002	Cy23r4–Cy24r3
2.	Apr 2002–Feb 2004	Cy25r1–Cy26r3
3.	Mar 2004–Aug 2006	Cy28r1–Cy30r1
4.	Sep 2006–May 2008	Cy31r1–Cy32r3
5.	Jun 2008–Dec 2009	Cy33r1–Cy35r3
6.	Jan 2010–Apr 2011	Cy36r1–Cy36r4

ACPD
14, 14399–14438, 2014

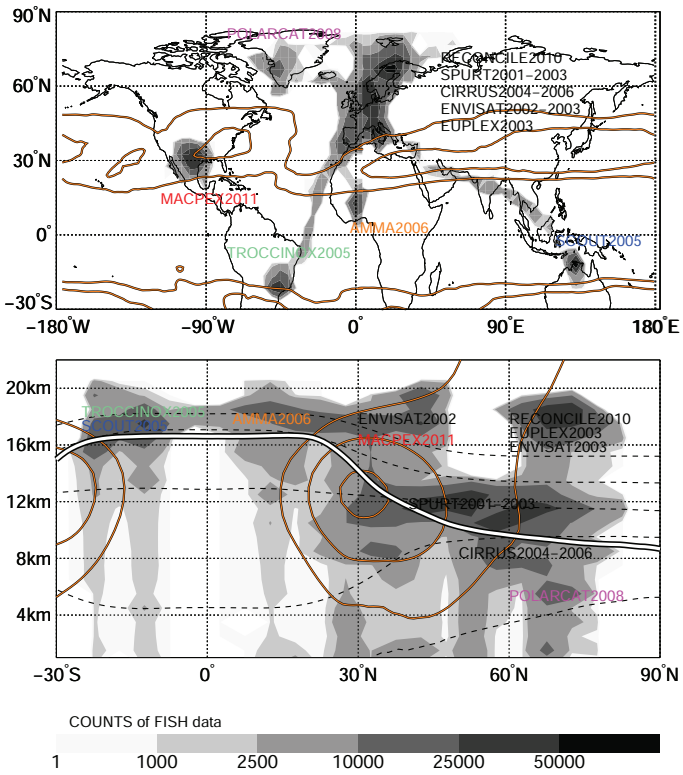

Figure 1. Latitude–longitude (top panel) and altitude–latitude (bottom panel) representation of FISH water vapor measurements. Counts of 1 Hz measurements are shown for 5° lat × 5° lon and 1 km × 5° lat bins, respectively. The measurement locations of the different campaigns are indicated in both panels. The ERA-Interim horizontal wind speed at 13 km (top panel) and as cross-section through all altitudes (lower panel) is shown as mean over all 136 flight mission days between 2001 and 2011. The mean ERA-Interim isentropic surfaces (290 K, 320 K, 350 K, 380 K, and 410 K) are black dashed lines, and the mean location of the thermal tropopause is given by a white solid line.

ACPD
14, 14399–14438, 2014

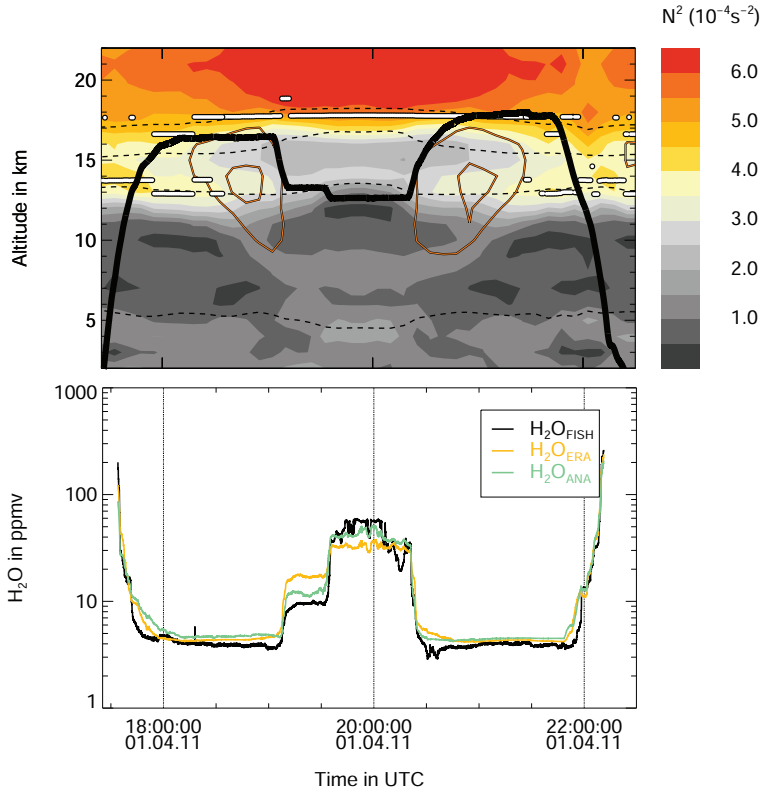

Figure 2. Example flight on 1 April 2011 during the MACPEX campaign over the US between 15–40° N. Top panel: altitude-time projection of ERA-Interim static stability (colored contours) along the flight path (black solid line). Isentropes (320 K, 350 K, 380 K, and 410 K) as black dashed lines, horizontal wind speed as orange lines, and thermal tropopause as white line. Lower panel: water vapor mixing ratio in ppmv measured by FISH (H_2O_{FISH}, black line) and ECMWF reanalysis (H_2O_{ERA}, orange line) and operational analysis water vapor mixing ratio (H_2O_{ANA}, green line).

ACPD
14, 14399–14438, 2014

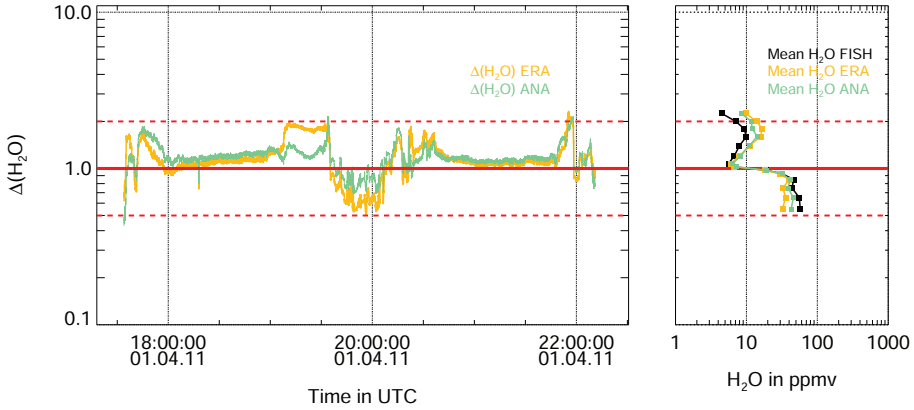

Figure 3. Left panel: the ratio $\Delta(H_2O)$ for the reanalysis (orange line) and the operational analysis water vapor (green line) for the example MACPEX flight on 1 April 2011 shown in Fig. 2. The red solid line marks a perfect agreement ($\Delta(H_2O) = 1$). The red dashed lines indicate the limits when the simulations are twice ($\Delta(H_2O) = 2$) or half ($\Delta(H_2O) = 0.5$) as high as the observations. Right panel: mean water vapor mixing ratio per $\Delta(H_2O)$ bin for H_2O_{FISH} (black line), H_2O_{ERA} (orange line), and H_2O_{ANA} (green line).

ACPD
14, 14399–14438, 2014

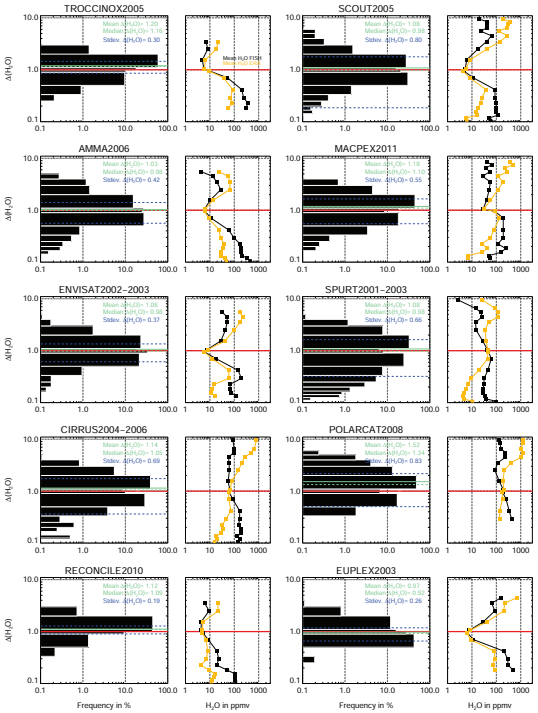

Figure 4. Left panels: frequency distribution of $\Delta(H_2O_{ERA})$ separately for each measurement campaign. Bin size of $\Delta(H_2O_{ERA})$ is organized according to [. . . , 0.25, 0.33, 0.5, 0.9, 1, 1.1, 2, 3, 4, . . .]. Only frequencies larger than 0.1 % are shown. The red solid line marks a perfect agreement ($\Delta(H_2O_{ERA})$ = 1). The mean of the distribution (green solid line), the median (green dashed line), and the standard deviation (blue dashed line) are also shown. Right panels: mean water vapor mixing ratio per $\Delta(H_2O_{ERA})$ bin for H_2O_{FISH} (black line) and H_2O_{ERA} (orange line).

ACPD
14, 14399–14438, 2014

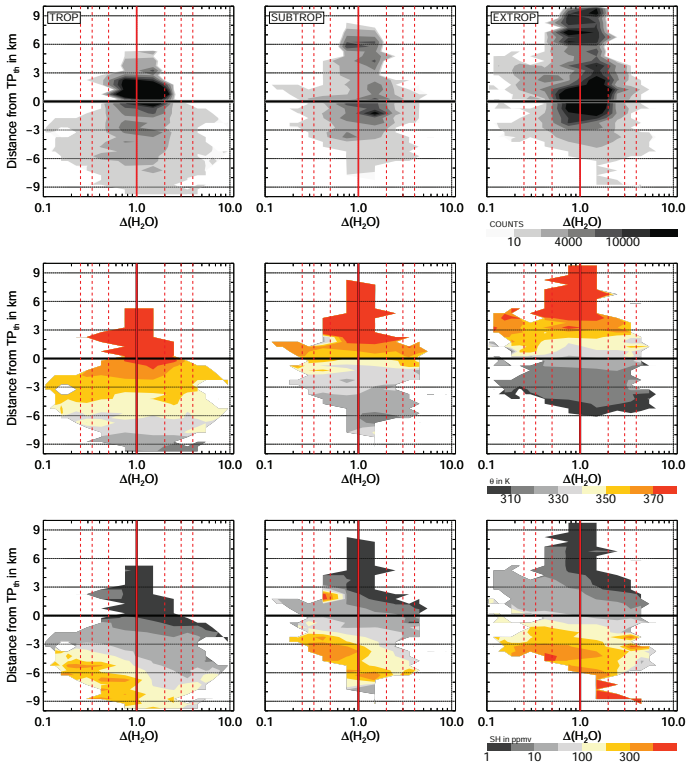

Figure 5. Counts of data, potential temperature, and water vapor for all measurement campaigns shown in Fig. 1 plotted in a $\Delta(H_2O_{ERA})$ and thermal tropopause related coordinate system. The distributions are shown for the tropical domain ($z_{TP} > 14$ km) (left), the subtropical (12 km $\leq z_{TP} \leq$ 14 km) (middle), and for the extratropical domain ($z_{TP} < 12$ km) (right). The red solid line marks a perfect agreement, i.e, $\Delta(H_2O_{ERA}) = 1$, and the red dashed lines mark a ratio $\Delta(H_2O_{ERA})$ between 0.25 and 4. Thermal tropopause bin size is 1 km and $\Delta(H_2O_{ERA})$ bins are organized as for Fig. 4.

ACPD
14, 14399–14438, 2014

UTLS water vapor comparison

A. Kunz et al.

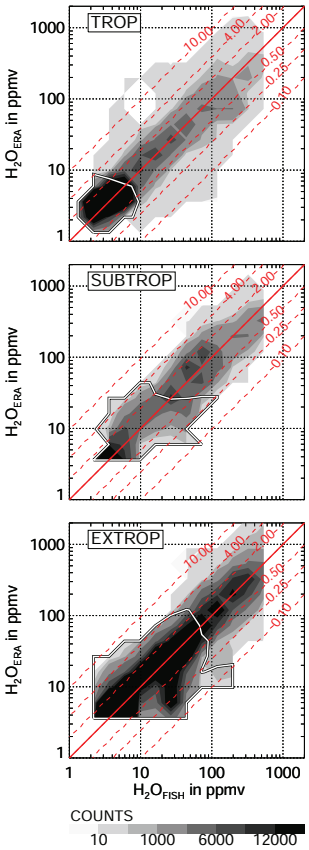

Figure 6. Correlation between H_2O_{ERA} and H_2O_{FISH}. Filled gray contours represent the counts of data within logarithmic H_2O bins. Red lines mark selected $\Delta(H_2O_{ERA})$ ratios and the white lines surround bins that are representative for the stratosphere.

ACPD
14, 14399–14438, 2014

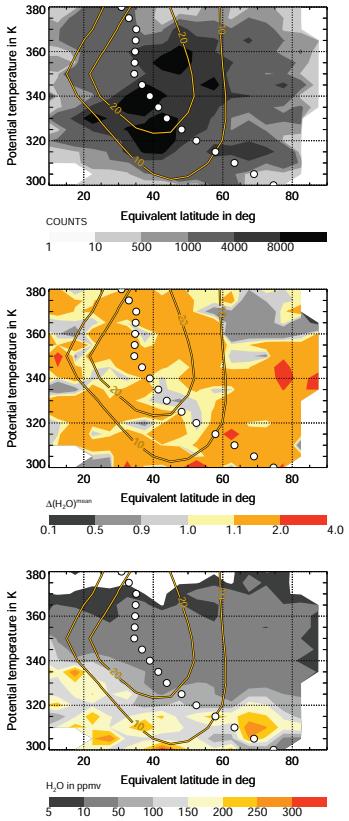

Figure 7. Counts of data (top panel), mean $\Delta(H_2O_{ERA})$ (middle panel) and mean H_2O_{FISH} (bottom panel) based on all Northern Hemisphere measurement campaigns (TROCCINOX and SCOUT are excluded) per 5 K potential temperature and 5° equivalent latitude bin. The equivalent latitude position of the dynamic tropopause (white circles) is shown on each isentrope as mean over all measurement days. Zonal mean zonal wind speed at all measurement days is represented by orange contours.

ACPD
14, 14399–14438, 2014

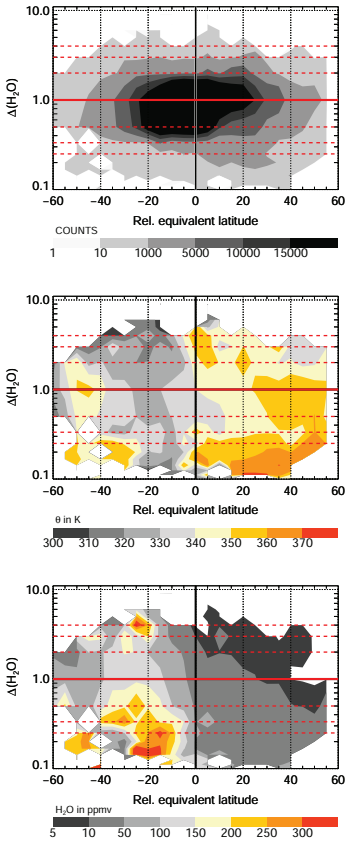

Figure 8. Counts of data (top panel), mean potential temperature (middle panel) and mean H_2O_{FISH} (bottom panel) of all Northern Hemisphere measurement campaigns (TROCCINOX and SCOUT are excluded) plotted as averages per logarithmic $\Delta(H_2O_{ERA})$ and 5° relative equivalent latitude difference bin with respect to the dynamic tropopause (see white circles in Fig. 7).

ACPD
14, 14399–14438, 2014

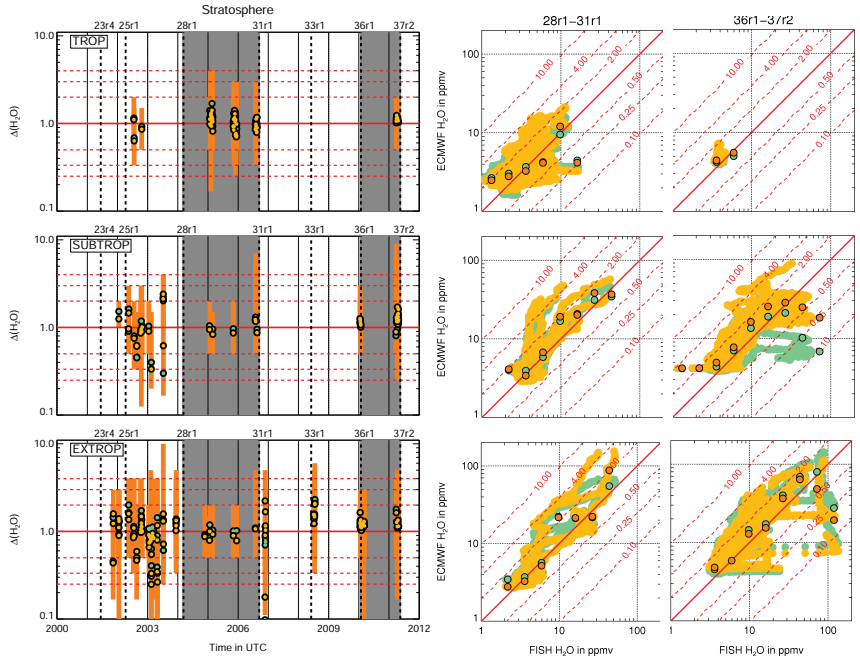

Figure 9. Left panels: daily mean $\Delta(H_2O)$ of operational analysis water vapor mixing ratio (H_2O_{ANA}, black-orange dots) over the time for stratospheric measurements in the tropical (top panel), subtropical (middle panel), and extratropical domain (bottom panel). The range between the minimum and maximum value of $\Delta(H_2O_{ANA})$ on each day is marked by the orange vertical bars, the daily mean $\Delta(H_2O_{ERA})$ by the black-green dots. Dashed red lines indicate $\Delta(H_2O)$ between 0.33 and 3, black dashed lines indicate the dates when selected IFS Cycles became operational. Right panels: correlation of H_2O_{FISH} with H_2O_{ANA} (orange) and with H_2O_{ERA} (green) for two IFS Cycle time periods (gray shadings, left panels). The first period, i.e., IFS Cycles 28r1–31r1, include measurements from 9 March 2004 to 12 September 2006 and the second period, i.e., IFS Cycles 36r1–37r2, measurements from 26 January 2010 to 18 May 2011. Means per H_2O_{FISH} bin are shown by black-surrounded larger dots.

ACPD
14, 14399–14438, 2014

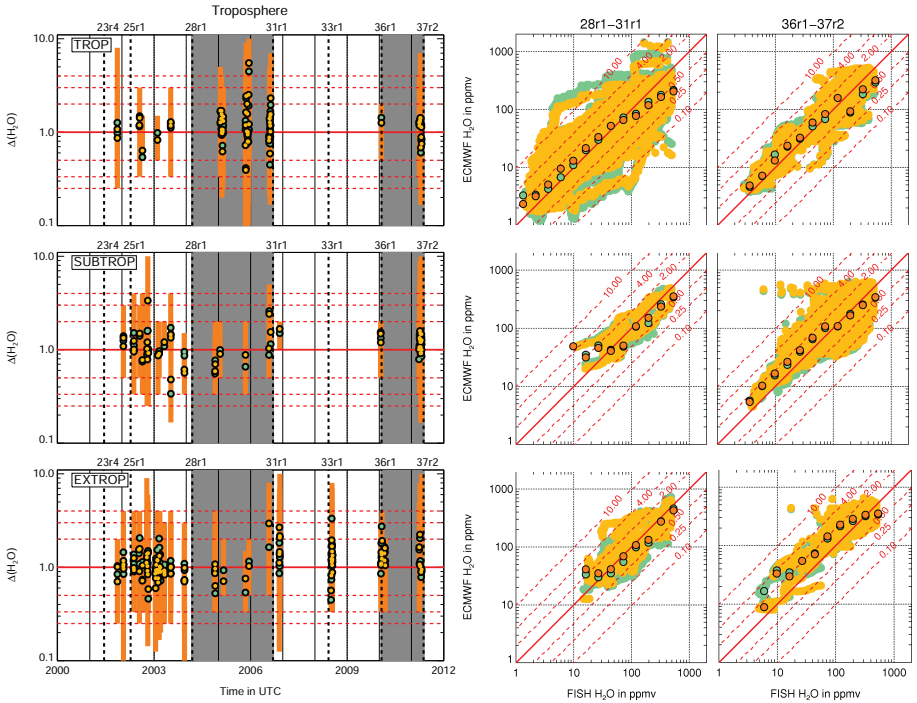

Figure 10. As Fig. 9 but for tropospheric measurements in the three different atmospheric domains.

ACPD
14, 14399–14438, 2014